The alternating current response of one-dimensional hot electrons in cylindrical quantum wires

1995 J. Phys.: Condens. Matter 7 8587

(http://iopscience.iop.org/0953-8984/7/45/014)

J. Phys.: Condens. Matter 7 (1995) 8587–8596. Printed in the UK

The alternating current response of one-dimensional hot electrons in cylindrical quantum wires

Z Q Zou and X L Lei

China Centre of Advanced Science and Technology (World Laboratory), PO Box 8730, Beijing 100080, People's Republic of China and Shanghai Institute of Metallurgy, Chinese Academy of Sciences, 865 Changning Road, Shanghai 200050, People's Republic of China

Received 8 June 1995, in final form 31 July 1995

Abstract. Linear ac transport of a one-dimensional electron gas in cylindrical GaAs quantum wires (QWs) under zero to moderate dc bias fields has been examined on the basis of the balance equation transport theory. Dynamic screening of the electron–electron interaction is considered in the random phase approximation. In contrast to the case without a dc bias field, the ac mobility contains an additional contribution from the electron temperature oscillation when a dc bias field is simultaneously applied. Numerical results at 4.2 K show that the plasma contributions noticeably change the memory functions even with a dc bias of moderate strength. As a result, the ac mobility is appreciably influenced by the plasma excitation at frequency ranging from 1 GHz to 30 GHz.

1. Introduction

Hot-electron transport in quantum wires (QWs) is currently the subject of increasing interest for their potential application in electronic devices. Linear and high-field dc conductions in square and cylindrical systems have been analysed in great detail in the literature [1–5]. The examination of the high-frequency ac response in QWs has also been given attention. Recently, Basu and coworkers [6] reported a theoretical investigation on small-signal mobility of hot electrons moving one dimensionally in GaAs and $In_{0.53}Ga_{0.47}As$ square QWs at low temperature when a high-frequency electric field is superimposed on a dc bias field of varying strength. For two-dimensional (2D) and three-dimensional (3D) bulk materials a good understanding of dynamic conductivity has been achieved through the extensive study in the the past twenty years [7–15]. It is believed that the electron plasma modes play an important role at low lattice temperature when only a weak-signal ac electric field is applied [10–14]. When a strong dc electric field is simultaneously biased, although the rise of the electron temperature suppresses the contribution of the electron plasma excitation to the ac response of the system, the oscillation of the electron temperature may strongly affect the behaviour of the ac mobility at low frequency for the parallel configuration [9, 14]. These two mechanisms could also show up in the dynamic conductivity of a QW system. The electron collective excitation spectra of one-dimensional QWs have been explored theoretically by Gold and Ghazali [16], Wendler and coworkers [17] and Li and Das Sarma [18], and experimentally by Demel *et al* [19]. In contrast to 3D electron systems, the plasma frequency of a one-dimensional (1D) electron gas starts from zero and the spectrum exhibits a logarithmic dispersion at small wave vectors. This suggests that the electron plasma excitations may play an even more important role in a

0953-8984/95/458587+10$19.50

1D quantum wire system than in a 3D bulk. In this paper, we explore the high-frequency response of GaAs QWs under a dc bias field of varying strength, with attention focused on the effects of electron collective excitation and electron temperature oscillation. Since the effect of the plasma excitation is expected to be important when electron temperature is not too high, we concentrate here mainly on the case of low lattice temperature and low to moderate bias voltage. We find a significant plasma-mode-induced contribution to the imaginary part of the memory function throughout a frequency range of more than four orders of magnitude, leading to an appreciable change in the ac mobility with or without a dc bias. Furthermore, we find a strong effect of the electron temperature oscillation in QWs, which greatly suppresses the ac mobility at low frequency.

2. Model QW and ac mobility

We consider a cylindrical model quantum wire. The electrons, moving along the wire of length L in the z direction and quantized laterally in the $r_\parallel = (r_\parallel, \phi)$ plane within a range of radius ϱ, are scattered by randomly located impurities and coupled with phonons. For moderate bias voltages and temperatures considered in this paper, the separation between the lowest and the next-higher subband is much larger than the maximum average electron energy. The electrons are, therefore, supposed to occupy only the lowest subband. Assuming an infinite potential barrier at $r_\parallel = \varrho$ and using cylindrical coordinates $(r_\parallel, \phi, z)$, we have the ϕ-unrelated electron wave function of the form

$$\psi_{k_z}(r_\parallel, z) = \varphi(r_\parallel)\frac{\exp(ik_z z)}{\sqrt{L}} = \frac{1.087}{\varrho} J_0\left(\frac{2.405}{\varrho} r_\parallel\right)\frac{\exp(ik_z z)}{\sqrt{L}} \tag{1}$$

with the energy counted from the conduction-band bottom $\varepsilon(k_z) = k_z^2/2m$. Here k_z is the one-dimensional wave vector, m is the electron effective mass and J_0 is the zeroth-order Bessel function.

Assuming that elastic scattering is due to randomly distributed charge impurities and that electrons are coupled to 3D bulk phonons, we can express the matrix elements for electron–impurity and electron–phonon scatterings in terms of the above QW electron wave function as $U(q)F(q_\parallel)$ and and $M(q, \lambda)F(q_\parallel)$. Here $U(q)$ is the impurity potential and $M(q, \lambda)$ is the electron–phonon coupling matrix element in the 3D Fourier representation. $F(q_\parallel)$ is a form factor of the quasi-1D electron system with the expression

$$F(q_\parallel) = 7.421 \int_0^1 \zeta \, d\zeta \; J_0^2(2.405\zeta) J_0(q_\parallel \varrho \zeta). \tag{2}$$

We can also obtain the matrix elements of the intercarrier Coulomb interaction as

$$V(q_z) = \frac{e^2}{2\pi\epsilon_0 \kappa L} \int dr_\parallel \, dr'_\parallel \, |\varphi(r_\parallel)|^2 |\varphi(r'_\parallel)|^2 K_0(|q_z||r_\parallel - r'_\parallel|) \tag{3}$$

where K_0 is the modified Bessel function of zeroth order, κ is the high-frequency dielectric constant of the quantum wire material, $q_\parallel$ represents the lateral wave vector and $q = (q_\parallel, q_z)$.

A numerical test shows that the Coulomb matrix element (3) can be replaced by the following expressions with sufficient accuracy:

$$V(q_z) = \frac{18e^2}{\pi\epsilon_0\kappa(q_z\varrho)^2}\left[\frac{1}{10} - \frac{2}{3(q_z\varrho)^2} + \frac{32}{3(q_z\varrho)^4} - \frac{64}{(q_z\varrho)^4} I_3(q_z\varrho) K_3(q_z\varrho)\right] \tag{4}$$

(I_3 and K_3 are the modified Bessel functions of order three) for $|q_z|\varrho > 0.2$, and

$$V(q_z) = -\frac{e^2}{2\pi\epsilon_0\kappa}\left\{\ln\left(\frac{\nu|q_z|\varrho}{2}\right) - 0.6083 + (q_z\varrho)^2\left[\frac{1}{8}\ln\left(\frac{\nu|q_z|\varrho}{2}\right) - 0.1450\right]\right\} \tag{5}$$

($\nu = 1.781$ is the Euler constant) for $|q_z|\varrho < 0.2$. These expressions have been used in the electron plasma analyses [16, 17]. To save computing time, we will use equations (4) and (5) to evaluate the matrix element of the Coulomb interaction in the following numerical calculation.

The high-frequency response of a QW under a dc bias can be conveniently investigated within the framework of the balance equation theory [20, 21]. We consider a small-amplitude ac signal electric field $2E_1 \cos \omega t$ applied along the wire (z direction), together with a moderate dc bias field E_0:

$$E(t) = E_0 + E_1 e^{-i\omega t} + E_1 e^{i\omega t}. \tag{6}$$

In the oscillatory steady state the centre of mass moves at a constant drift velocity v_d and oscillates with a small amplitude at the single driving frequency ω,

$$v(t) = v_d + v_1 e^{-i\omega t} + v_1^* e^{i\omega t} \tag{7}$$

and the electron temperature $T_e(t)$ will also oscillate about a constant value T_e,

$$T_e(t) = T_e + T_1 e^{-i\omega t} + T_1^* e^{i\omega t}. \tag{8}$$

These, to leading order in the small quantities, provide the line densities of the frictional force $f = f_i + f_p$ (due to impurity and phonon scatterings), and of the energy transfer rate w (due to phonon scattering) with the following expressions:

$$f = f_0 + f_0^{(1)}(T_1 e^{-i\omega t} + T_1^* e^{i\omega t}) + (f_1 e^{-i\omega t} + f_1^* e^{i\omega t}) \tag{9}$$

$$w = w_0 + w_0^{(1)}(T_1 e^{-i\omega t} + T_1^* e^{i\omega t}) + (w_1 e^{-i\omega t} + w_1^* e^{i\omega t}). \tag{10}$$

Here $f_0 = f_0(v_d, T_e)$ and $w_0 = w_0(v_d, T_e)$ are the force- and energy-transfer rate expressions in the dc steady state [11, 20] with drift velocity v_d and electron temperature T_e; $f_0^{(1)} \equiv \partial f_0(v_d, T_e)/\partial T_e$ and $w_0^{(1)} \equiv \partial w_0(v_d, T_e)/\partial T_e$. $f_1 = f_1(\omega, v_d, T_e)$ and $w_1 = w_1(\omega, v_d, T_e)$ are frequency-dependent linear-order small quantities related to the memory effect. Their zero-frequency values are just $f_1(0, v_d, T_e) = v_1 \partial f_0(v_d, T_e)/\partial v_d$ and $w_1(0, v_d, T_e) = v_1 \partial w_0(v_d, T_e)/\partial v_d$. For their full expressions please refer to [12] and [20].

Following the balance equation treatment of [14], we can easily obtain the complex small-signal ac mobility under a dc bias to be

$$\mu(\omega, v_d) \equiv \frac{v_1}{E_1} = \frac{ie}{m} \frac{1}{\omega + M(\omega, v_d) + D(\omega, v_d)} \tag{11}$$

with

$$D(\omega, v_d) = -\frac{v_d f_0^{(1)}[M(\omega, v_d) + N(\omega, v_d) + i\tau_0^{-1}]}{v_d f_0^{(1)} + w_0^{(1)} - i\omega C_e}. \tag{12}$$

Here $D(\omega, v_d)$ is a quantity reflecting the effect of the electron temperature oscillation. $\tau_0^{-1} = -f_0/n_1 m v_d$ is the effective inverse scattering time related to the dc nonlinear resistivity at the bias field. n_1 is the electron wire density. C_e is the specific heat of the electron system at the bias electron temperature T_e. $M(\omega, v_d)$ is the momentum-related memory function, which consists of contributions from impurities, $M^i(\omega, v_d)$, and from phonons, $M^p(\omega, v_d)$. $N(\omega, v_d)$ is the energy-related memory function. The expressions of $M(\omega, v_d)$ and $N(\omega, v_d)$ have the following forms:

$$M^i(\omega, v_d) = \frac{n_i}{n_1 m \omega} \sum_q |U(q)|^2 |F(q_\parallel)|^2 q_z^2 \left[\Pi(q_z, q_z v_d) - \Pi(q_z, q_z v_d + \omega)\right] \tag{13}$$

$$M^p(\omega, v_d) = \frac{1}{n_1 m \omega} \sum_{q,\lambda} |M(q, \lambda)|^2 |F(q_\parallel)|^2 q_z^2 \left[\Lambda(q, \lambda, q_z v_d) - \Lambda(q, \lambda, q_z v_d + \omega)\right] \tag{14}$$

$$N(\omega, v_d) = \frac{1}{n_1 m \omega v_d} \sum_{q,\lambda} |M(q,\lambda)|^2 |F(q_\parallel)|^2 q_z \Omega_{q\lambda} \left[\Gamma(q,\lambda,q_z v_d) - \Gamma(q,\lambda,q_z v_d + \omega)\right] \tag{15}$$

where $\Omega_{q\lambda}$ is the phonon energy, n_i is the bulk density of impurities, $\Pi(q_z,\omega)$ is the one-dimensional electron density–density correlation function including the Coulomb interaction and $\Lambda(q,\lambda,\omega)$ and $\Gamma(q,\lambda,\omega)$ are electron–phonon correlation functions. For the one-subband model, $\Pi(q_z,\omega)$ can be expressed under the random phase approximation in the form

$$\Pi(q_z,\omega) = \frac{\Pi_0(q_z,\omega)}{1 - v(q_z)\Pi_0(q_z,\omega)} \tag{16}$$

and $\Pi_0(q_z,\omega)$ is the 1D electron density–density correlation function (per unit length) in the absence of the Coulomb interaction,

$$\Pi_0(q_z,\omega) = 2\sum_{k_z} \frac{f(\varepsilon(k_z)) - f(\varepsilon(k_z+q_z))}{\omega + \varepsilon(k_z) - \varepsilon(k_z+q_z) + \mathrm{i}\delta} \tag{17}$$

where $f(\varepsilon) = \{\exp(\varepsilon - \varepsilon_f)/T_e + 1\}^{-1}$ is the Fermi distribution and ε_f is the chemical potential determined by the electron wire density

$$n_1 = 2\sum_{k_z} f(\varepsilon(k_z)). \tag{18}$$

At zero electron temperature $T_e = 0$ K, the real and imaginary parts of $\Pi_0(q_z,\omega)$ are given, respectively, by the following analytical expressions:

$$\Pi_{01}(q_z,\omega) = \frac{m}{\pi q_z} \ln\left|\frac{(m\omega/q_z)^2 - (q_z/2 - k_F)^2}{(m\omega/q_z)^2 - (q_z/2 + k_F)^2}\right| \tag{19}$$

$$\Pi_{02}(q_z,\omega) = \frac{m}{|q_z|}\left\{\Theta\left[k_F^2 - \left(\frac{q_z}{2} + \frac{m\omega}{q_z}\right)^2\right] - \Theta\left[k_F^2 - \left(\frac{q_z}{2} - \frac{m\omega}{q_z}\right)^2\right]\right\}. \tag{20}$$

Here $k_F = \pi n_1/2$ is the zero-temperature Fermi wave vector and $\Theta(x)$ is the unit-step function. In terms of the real part $\Pi_1(q_z,\omega)$ and the imaginary part $\Pi_2(q_z,\omega)$ of the correlation function $\Pi(q_z,\omega)$, the imaginary and real parts of the correlation function $\Lambda(q,\lambda,\omega)$ can be expressed as

$$\begin{aligned}\Lambda_2(q,\lambda,\omega) = {} & \Pi_2(q_z,\omega - \Omega_{q\lambda})\left[n\left(\frac{\Omega_{q\lambda}}{T_L}\right) - n\left(\frac{(\Omega_{q\lambda} - \omega)}{T_e}\right)\right] \\ & + \Pi_2(q_z,\omega + \Omega_{q\lambda})\left[n\left(\frac{\Omega_{q\lambda}}{T_L}\right) - n\left(\frac{(\Omega_{q\lambda} + \omega)}{T_e}\right)\right]\end{aligned} \tag{21}$$

and

$$\begin{aligned}\Lambda_1(q,\lambda,\omega) = {} & \left[\Pi_1(q_z,\omega - \Omega_{q\lambda}) + \Pi_1(q_z,\omega + \Omega_{q\lambda})\right] n\left(\frac{\Omega_{q\lambda}}{T_L}\right) \\ & - \frac{1}{\pi}\int_{-\infty}^{+\infty} \mathrm{d}\omega_1\, \Pi_2(q_z,\omega_1) n\left(\frac{\omega_1}{T_e}\right)\left[\frac{1}{\omega_1 + \omega - \Omega_{q\lambda}} + \frac{1}{\omega_1 - \omega - \Omega_{q\lambda}}\right]\end{aligned} \tag{22}$$

and the imaginary and real parts of the correlation function $\Gamma(q,\lambda,\omega)$ can be written as

$$\begin{aligned}\Gamma_2(q,\lambda,\omega) = {} & \Pi_2(q_z,\omega + \Omega_{q\lambda})\left[n\left(\frac{\Omega_{q\lambda}}{T_L}\right) - n\left(\frac{(\Omega_{q\lambda} + \omega)}{T_e}\right)\right] \\ & - \Pi_2(q_z,\omega - \Omega_{q\lambda})\left[n\left(\frac{\Omega_{q\lambda}}{T_L}\right) - n\left(\frac{(\Omega_{q\lambda} - \omega)}{T_e}\right)\right]\end{aligned} \tag{23}$$

and

$$\Gamma_1(q,\lambda,\omega) = \left[\Pi_1(q_z,\omega+\Omega_{q\lambda}) - \Pi_1(q_z,\omega-\Omega_{q\lambda})\right] n\left(\frac{\Omega_{q\lambda}}{T_L}\right) + \frac{1}{\pi}\int_{-\infty}^{+\infty} d\omega_1\, \Pi_2(q_z,\omega_1) n\left(\frac{\omega_1}{T_e}\right)\left[\frac{1}{\omega_1+\omega-\Omega_{q\lambda}} - \frac{1}{\omega_1-\omega-\Omega_{q\lambda}}\right] \quad (24)$$

where $n(x) = 1/[\exp(x) - 1]$ is the Bose function and T_L is the lattice temperature.

In the absence of a dc bias $E_0 = 0$, one can obtain $T_1 = 0$ from the zero-order balance equation and the linear-order ac energy balance equation [14], which means that the electron temperature remains undamped to linear order in the signal and any change of the electron temperature must be of higher order. We thus have $D(\omega, 0) = 0$.

Electron plasma modes in QWs have been analysed in detail in the literature [16–19] based on the electron density correlation function (17). The plasma frequency of a 1D electron system starts from zero and the spectrum exhibits a logarithmic dispersion at small wave vectors. These plasma modes, which greatly affect the spectrum of the electron density correlation $\Pi(q_z, \omega)$, could also give rise to a significant contribution to the memory functions $M^i(\omega, v_d)$, etc, and thus have an important influence on the high-frequency response of a QW.

3. Numerical results and discussion

We consider n-doped GaAs cylindrical QWs with radius $\varrho = 5$ nm. The impurity concentration is taken as $n_i = 10^{22}$ m^{-3}, the same as that in [6]. The wire densities of the conduction electron are chosen to be $n_1 = 9.6 \times 10^7$ and 4.8×10^7 m^{-1}, with zero-temperature Fermi temperatures $T_F = 150.1$ and 37.5 K, respectively. The material parameters for GaAs are taken from [22] and shown in table 1.

Table 1. Values of material parameters used in computations.

Effective mass m (m_0)	0.067
Static dielectric constant κ	12.8
Optic dielectric constant κ_∞	10.9
Mass density d (kg m^{-3})	5.15×10^3
Acoustic deformation potential Ξ (eV)	8.6
Piezoelectric constant e_{14} (V m^{-1})	1.44×10^9
Longitudinal optical phonon energy Ω_{LO} (meV)	35.4
Longitudinal sound velocity v_{sl} (m s^{-1})	5.22×10^3
Transverse sound velocity v_{st} (m s^{-1})	2.48×10^3

Because the plasma effect should be the strongest at lowest temperature, we consider first the situation when only a weak ac electric field is applied at low lattice temperature ($T_L = 4.2$ K). The effect due to electron temperature oscillation vanishes in the case of zero dc bias.

The imaginary part of the impurity-induced memory function without a dc bias, $M_2^i(\omega, 0)$, is plotted as a function of frequency $\nu = \omega/2\pi$ of the driving ac field in figure 1, together with the real part of the ac mobility $\mu_1(\omega, 0)$ (inset). The solid curves are obtained by including contributions from the plasma modes and the dashed curves by excluding them. The plasma contribution in QWs is much more significant than that in 3D systems [14]. It starts from very low frequency and exhibits large and broad humps. In the case of $n_1 = 9.6 \times 10^7$ m^{-1}, the plasma-induced contribution constitutes 1.4% of $M_2^i(\omega, 0)$

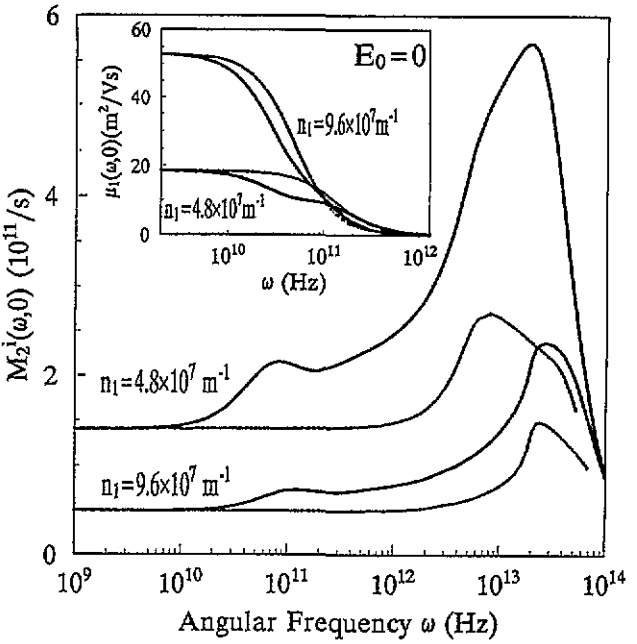

Figure 1. The imaginary part of the impurity-induced memory function for a GaAs cylindrical QW with $\varrho = 5$ nm at $T_L = 4.2$ K and zero dc bias, $M_2^i(\omega, 0)$, is shown as a function of frequency $\nu = \omega/2\pi$ at two electron wire densities $n_1 = 4.8 \times 10^7$ m^{-1} and $n_1 = 9.6 \times 10^7$ m^{-1}. The inset displays the variation of the real part of the ac mobility of the QW, $\mu_1(\omega, 0)$, with frequency. The solid curves include the contribution from plasma excitations and the dashed curves exclude that.

at $\nu = 2$ GHz and increases to the maximum 38.4% at $\nu = 4.4$ THz. In the case of $n_1 = 4.8 \times 10^7$ m^{-1}, the contribution due to plasma excitation constitutes 3.2% of $M_2^i(\omega, 0)$ at $\nu = 2$ GHz and increases to the maximum 57.4% at $\nu = 2.8$ THz. This indicates the fact that the role of the single-particle excitation of the electron gas decreases and the collective excitation plays a more important role with decreasing electron wire density. The inset shows that the effect of the plasma excitation on the ac mobility is also quite significant for frequency higher than 1 GHz.

When a dc bias field is simultaneously applied, a small ac current parallel to the dc bias field will induce an energy (thus an electron temperature) change in linear order in order to satisfy the force and energy balance equations. The ac mobility $\mu(\omega, v_d)$ differs from $\mu(\omega, 0)$ without a dc bias not only due to $M(\omega, v_d)$ differing from $M(\omega, 0)$, but also due to the additional term $D(\omega, v_d)$ induced by the electron temperature oscillation. Figures 2–6 display the numerical results under different dc biases at lattice temperature $T_L = 4.2$ K for the case of $n_1 = 9.6 \times 10^7$ m^{-1}.

The computed imaginary part of the impurity-induced memory function $M_2^i(\omega, v_d)$ is plotted in figure 2 as a function of frequency under dc bias fields $E_0 = 0.2, 16.2, 59.6, 159.4$ and 284.3 V m^{-1}, corresponding to electron temperatures $T_e = 4.2, 5.6, 10.2, 20$ and 30 K and the bias drift velocities $v_d = 10, 760, 2.26 \times 10^3, 4.55 \times 10^3$ and 6.55×10^3 m s^{-1}. The solid curves include the contributions from the plasma excitation and the dashed curves exclude those. Similar to the case without a dc bias, the plasma-excitation-induced contribution to $M_2^i(\omega, v_d)$ is still significant for frequencies above 2 GHz. This contribution decreases with increasing dc bias field but not as fast as that in a 3D system [14]. Note

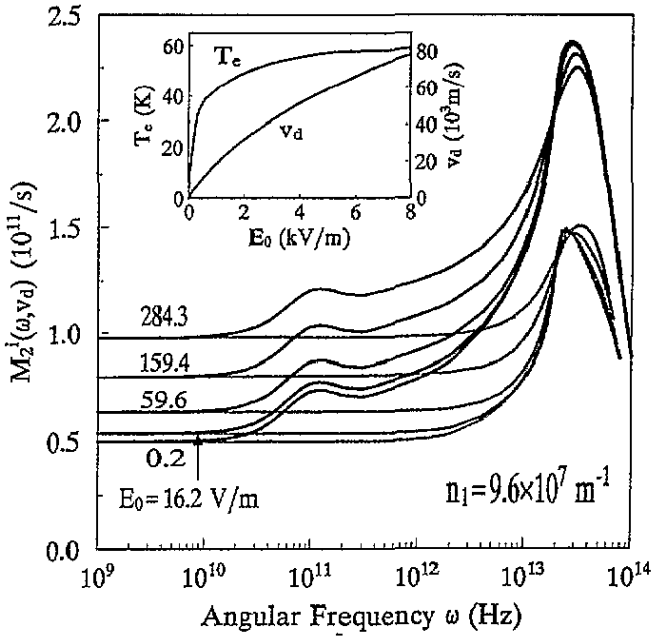

Figure 2. The imaginary part of the impurity-induced memory function, $M_2^i(\omega, v_d)$, is shown as a function of frequency $\nu = \omega/2\pi$ for the QW as described in figure 1 at $T_L = 4.2$ K and $n_1 = 9.6 \times 10^7$ m^{-1} under different dc biases. The bias fields are $E_0 = 0.2, 16.2, 59.6, 159.4$ and 284.3 V m^{-1}, corresponding to the electron temperatures $T_e = 4.2, 5.6, 10.2, 20$ and 30 K and the bias drift velocities $v_d = 10, 7.6 \times 10^2, 2.26 \times 10^3, 4.55 \times 10^3$ and 6.55×10^3 m s^{-1}. The solid curves include the contribution from plasma excitations and the dashed curves exclude that. The inset indicates the drift velocity v_d and the electron temperature T_e against the electric field E_0, as determined by zero-order balance equations.

that in contrast to bulk materials [14], in GaAs quantum wires $M_2^i(\omega, v_d)$ increases with increasing electron temperature (dc bias field) at low frequencies. This is due to the fact that at low temperatures the chemical potential of a QW increases with increasing electron temperature, while the chemical potential of a bulk system decreases with increasing electron temperature. In figure 3, we plot the $D(\omega, v_d)$ function as defined in (12), together with $M^i(\omega, v_d)$, for the case of $E_0 = 159.4$ V m^{-1}. Similar to the 3D electron system [14], the $D(\omega, v_d)$-related contribution to mobility in the QW is important at low frequencies. At high frequencies, the electron temperature cannot follow the rapid oscillation of the driving field. As a result, both the real part $D_1(\omega, v_d)$ and imaginary part $D_2(\omega, v_d)$ of this function approach zero.

The ac mobility $\mu(\omega, v_d)$ is easily obtained from the results of $M(\omega, v_d)$ and $D(\omega, v_d)$. Figures 4 and 5 display the real part $\mu_1(\omega, v_d)$ and imaginary part $\mu_2(\omega, v_d)$ of the ac mobility, respectively, as a function of frequency under different dc bias fields. The solid curves include the contributions from the plasma excitation and electron temperature oscillation; the dot–dashed curves exclude the electron temperature oscillation. As shown by the solid curves in figure 4, at low frequencies $\mu_1(\omega, v_d)$ is greatly suppressed by $D(\omega, v_d)$ under moderate dc bias fields. Correspondingly, $\mu_2(\omega, v_d)$ is drawn towards a negative value by this effect and reaches a minimum at frequencies $\nu \sim 0.3$–0.8 GHz under moderate dc biases, then increases with increasing frequency towards a maximum before it finally decreases to vanishing. This phenomenon, though it also exists in 3D systems under

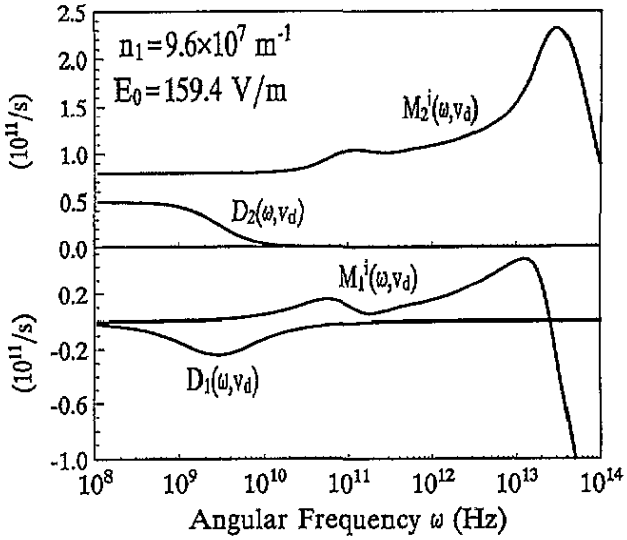

Figure 3. Real and imaginary parts of $D(\omega, v_d)$ and the impurity-induced memory function $M^i(\omega, v_d)$, for the GaAs QW at $n_1 = 9.6 \times 10^7$ m^{-1}, are shown as functions of frequency $\nu = \omega/2\pi$ under the bias field $E_0 = 159.4$ V m^{-1} ($T_e = 20$ K, $v_d = 4.55 \times 10^3$ m s^{-1}).

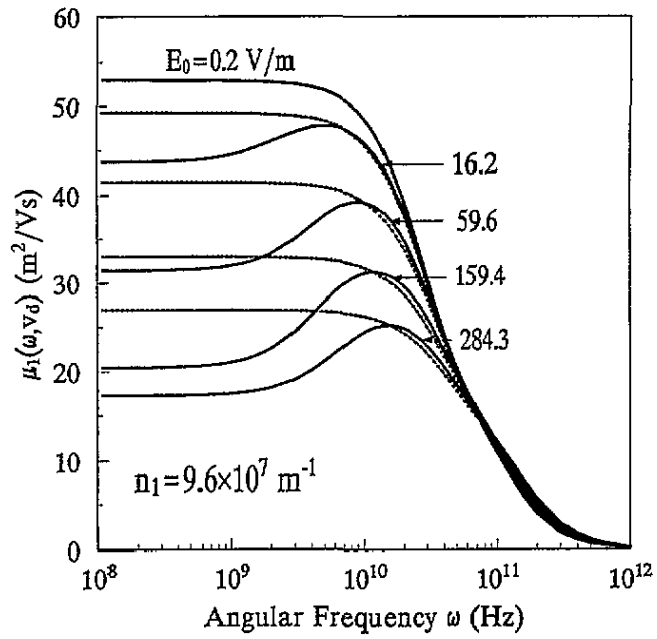

Figure 4. Variation of the real part of the ac mobility $\mu_1(\omega, v_d)$ with frequency $\nu = \omega/2\pi$ for the GaAs QW at $n_1 = 9.6 \times 10^7$ m^{-1} under dc bias fields $E_0 = 0.2$, 16.2, 59.6, 159.4 and 284.3 V m^{-1}. The solid curves include the contribution from the plasma excitation and the electron temperature oscillation, the dot–dashed curves exclude the latter.

a strong dc bias [9, 14, 15], is more pronounced and occurs at a relatively low dc bias in QWs. For the given carrier concentration and wire radius, both $\mu_1(\omega, v_d)$ and $\mu_2(\omega, v_d)$ are generally lower at higher dc bias than at lower dc bias due to the hot-electron nonlinearity.

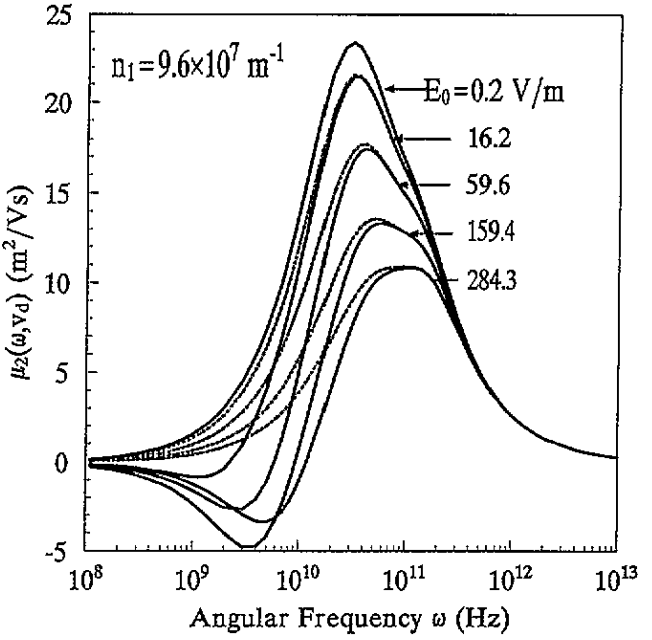

Figure 5. Variation of the imaginary part of the ac mobility $\mu_2(\omega, v_d)$ with frequency $\nu = \omega/2\pi$ for the GaAs QW at $n_1 = 9.6 \times 10^7$ m^{-1} under dc bias fields $E_0 = 0.2, 16.2, 59.6, 159.4$ and 284.3 V m^{-1}. The solid curves include the contribution from the plasma excitation and the electron temperature oscillation, the dot–dashed curves exclude the latter.

To show the effect of plasma excitations on the ac mobility while a dc bias field is applied, we plot in figure 6 $\mu_1(\omega, v_d)$ and $\mu_2(\omega, v_d)$ at dc bias field $E_0 = 159.4$ V m^{-1} as a function of frequency. The solid curves are results including the plasma contribution and the dashed curves exclude that. Neglect of the plasma contribution seems not to be a good approximation at least up to this strength of the bias field.

In conclusion, the high-frequency responses of GaAs cylindrical quantum wires are investigated at different dc biases by assuming that electrons are confined to the lowest subband. Particular attention has been paid to the effects of plasma excitation and electron temperature oscillation. We find that in QWs the electron plasma excitations noticeably enhance the memory effect and give rise to an appreciable influence on the high-frequency ac mobility at low lattice temperatures up to a moderate strength of the bias field, and that the electron temperature oscillation plays an important role at low frequencies when a moderate dc bias field is simultaneously applied. Although the experimental observation of the plasma effect requires the detailed analysis of the frequency and density dependence of the real and the imaginary parts of the complex mobilities, the remarkable humps showing up in the $\mu(\omega)$ versus ω curves in the presence of a dc bias should be easily detectable. These humps would not disappear even at high lattice temperature.

Acknowledgments

The authors thank the Chinese National Natural Science Foundation and the China National and Shanghai Municipal Commissions of Science and Technology for support of this work.

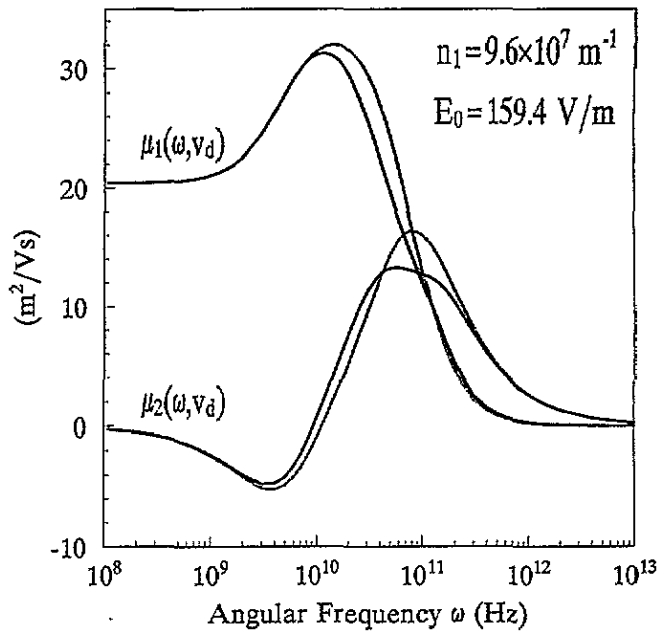

Figure 6. Variation of the real part $\mu_1(\omega, v_d)$ and imaginary part $\mu_2(\omega, v_d)$ of the ac mobility with frequency for the GaAs QW at $n_1 = 9.6 \times 10^7$ m^{-1} under the dc bias $E_0 = 159.4$ V m^{-1}. The solid curves include the contribution from plasma excitations and the dashed curves exclude that.

References

[1] Yamada T and Sone J 1989 *Phys. Rev.* B **40** 6265
[2] Ismail K, Antoniadis D A and Smith H I 1989 *Appl. Phys. Lett.* **54** 1130
[3] Hu G Y and O'Connell R F 1990 *Phys. Rev.* B **42** 8947
[4] Kim K W, Stroscio M A, Bhatt A, Mickevicius R and Mitin V V 1991 *J. Appl. Phys.* **70** 319
[5] Wang X F and Lei X L 1993 *Phys. Rev.* B **47** 16612; 1993 *Phys. Status Solidi* b **175** 433
[6] Basu P P, Chattopadhyay D and Rakshit P C 1992 *Phys. Rev.* B **46** 13254
[7] Götze W and Wöfle P 1976 *Phys. Rev.* B **6** 1226
[8] Kennedy T A, Wagner R J, McCombe B D and Tsui D C 1975 *Phys. Rev. Lett.* **35** 1109
[9] Das P and Ferry D K 1976 *Solid State Electron.* **19** 851
[10] Ting C S, Ganguly A K and Lai W Y 1981 *Phys. Rev.* B **24** 3371
[11] Lei X L and Zhang J Q 1986 *J. Phys. C: Solid State Phys.* **19** L73
Lei X L and Horing N J M 1986 *Phys. Rev.* B **33** 1912
[12] Cai W, Hu P, Zheng T F, Yudanin B and Lax M 1989 *Phys. Rev.* B **40** 7671
[13] Ma S-K and Shung K W-K 1993 *Phys. Rev.* B **48** 10751
[14] Zou Z Q and Lei X L 1995 *Phys. Rev.* B **51** 9493
[15] Weng X M and Lei X L 1995 *Phys. Status Solidi* b **187** 579
[16] Gold A and Ghazali A 1990 *Phys. Rev.* B **41** 7626
[17] Wendler L, Haupt R and Pechstedt R 1991 *Phys. Rev.* B **43** 14669
Wendler L and Grigoryan V G 1994 *Phys. Status Solidi* b **181** 133
[18] Li Qiang and Das Sarma S 1989 *Phys. Rev.* B **40** 5860
[19] Demel T, Heitmann D, Grambow P and Ploog K 1988 *Phys. Rev.* B **38** 12732; 1991 *Phys. Rev. Lett.* **66** 2657
[20] Lei X L and Ting C S 1984 *Phys. Rev.* B **30** 4809; 1985 *Phys. Rev.* B **32** 1112
[21] Lei X L and Horing N J M 1992 *Int. J. Mod. Phys.* **6** 805
[22] Lei X L, Birman J L and Ting C S 1985 *J. Appl. Phys.* **58** 2270